Integrated reflectivity measurements of hydrogen phthalate crystals for high-resolution soft x-ray spectroscopy

Article *in* Journal of Instrumentation · September 2014

DOI: 10.1088/1748-0221/9/09/P09008

CITATION
1

READS
741

2 authors:

Ulf Zastrau
European XFEL
117 PUBLICATIONS **3,798** CITATIONS

SEE PROFILE

Eckhart Foerster
Friedrich Schiller University Jena
394 PUBLICATIONS **9,482** CITATIONS

SEE PROFILE

Preprint typeset in JINST style - HYPER VERSION

Integrated reflectivity measurements of hydrogen phthalate crystals for high-resolution soft x-ray spectroscopy

Ulf Zastrau[a,b*] **and Eckhart Förster**[a,c]

[a] *Institut für Optik und Quantenelektronik (IOQ), Friedrich-Schiller-Universität Jena, Max-Wien Platz 1, 07743 Jena, Germany*
[b] *Stanford Linear Accelerator Center (SLAC), Menlo Park, CA 94025 U.S.A.*
[c] *Helmholtz Institut Jena, Fröbelstieg 3, 07743 Jena, Germany*

E-mail: ulf.zastrau@uni-jena.de

ABSTRACT: The integrated x-ray reflectivity of Potassium Hydrogen Phthalate (KAP) and Rubidium Hydrogen Phthalate (RAP) crystals is studied at a photon energy of $(1740 \pm 14)\,\mathrm{eV}$ using a double-crystal setup. The absolute measured reflectivities are in $< 5\%$ agreement with the values predicted by the dynamic diffraction theory for perfect crystals when absorption is included. Within 4% experimental error margins, specimen that were exposed to ambient conditions over many years show identical reflectivity as specimen that were cleaved just before the measurement. No differences are observed between cleaving off a $10\,\mu$m surface layer and splitting the entire crystal bulk of 2 mm thickness. We conclude that at $1.7\,\mathrm{keV}$ photon energy the penetration depth of $\sim 1\,\mu$m is large compared to a potentially deteriorated surface layer of a few 10 nm.

KEYWORDS: Spectrometers; Plasma diagnostics - interferometry, spectroscopy and imaging.

*Corresponding author.

Contents

1. Introduction

Recently, a number of scientific articles reported on the creation and diagnosis of a solid-density aluminum plasma with an X-ray free-electron laser [1, 2], direct measurements of the occurring ionization potential depression [3], and resonant Kα spectroscopy [4]. Further studies concern opacity effects in the solid-density plasma [5]. The employed experimental technique is emission spectroscopy of characteristic K-shell radiation in the photon energy range $E_{\mathrm{ph}} = 1480 - 2000\,\mathrm{eV}$ (wavelength $\lambda = 6.2 - 8.4\,\text{Å}$).

As dispersive elements, diffraction gratings and crystals with a lattice constant $2d > 9\,\text{Å}$ are of interest [6]. While reflection gratings have the advantage of suppressing harder x-rays, (allowing spectroscopy of soft x-rays in the presence of hard x-rays) crystals offer much better spectral resolution. All the studies cited above were performed using a flat crystal of ammonium dihydrogen phosphate (ADP) in orientation (101). Other useful crystals are Beryl ($Be_3Al_2(SiO_3)_6$), polyethylen terphthalate (PET), muscovite (mica) [7], and hydrogen phthalates [8]. Hydrogen phthalate crystals are hygroscopic, and their surface deteriorates [9] with time when exposed to ambient conditions. Mica and phthalate crystals have the advantage that thin sheets can be easily cleaved, which is of interest for at least two reasons: First, thin cleaved sheets can be bent, allowing the preparation of concentrating or imaging x-ray optics [10, 11, 12, 13, 14]. Second, by cleavage one can prepare a fresh crystal surface shortly before the experiment.

In this paper, the integrated x-ray reflectivity for single crystals of Potassium Hydrogen Phthalate (KAP) and Rubidium Hydrogen Phthalate (RAP) is measured at a photon energy of 1740 eV. We study the influence of fresh cleaved crystal surfaces as compared to specimen that were stored at ambient conditions for many years.

Table 1. Characteristic x-ray Kα lines of silicon (Z=14) according to Ref. [18].

line	transition	photon energy [eV]	line width [eV]	wavelength [Å]
Kα_1	KL_3	1739.98 ± 0.02	0.49	7.1255
Kα_2	KL_2	1739.38 ± 0.02	0.49	7.1280

2. Method

The most elegant approach to determine a flat crystal's reflection curve employs a pair of identical crystals mounted in parallel positions to constitute a double-crystal diffractometer [16, 17]. Using x-rays with sufficiently small divergence and spectral width, the setup is dispersion-free and the reflection curve of the second crystal can be obtained by rocking it around its central Bragg angle while recording the reflected intensity with a stationary detector - hence the term *rocking curve*. Modifications of this so-called $(n,-n)$-geometry comprise anti-parallel configurations with identical or different crystal pairs, $(n,+n)$ or $(n,+m)$.

According to Compton and Allison [16], the intensity P reflected by the second crystal (indexed B) as a function of angular rocking ω around its central Bragg angle Θ_B can be calculated via

$$\begin{aligned} P(\omega) = \int_{-\phi}^{\phi} \int_{\lambda_{\min}}^{\lambda_{\max}} \int_{-\alpha}^{\alpha} d\alpha \, d\lambda d\phi \;\; & \cdot \, G(\alpha,\phi) \cdot J(\lambda-\lambda_0) \cdot \\ & \cdot C_A\left(\qquad \alpha - \frac{1}{2}\phi^2 \tan\Theta_A \; - \; (\lambda-\lambda_0)\frac{\partial\Theta_A}{\partial\lambda_0} \right) \cdot \\ & \cdot C_B\left(\pm\omega \mp \alpha - \frac{1}{2}\phi^2 \tan\Theta_B \; - \; (\lambda-\lambda_0)\frac{\partial\Theta_B}{\partial\lambda_0} \right) \end{aligned} \tag{2.1}$$

Here, the angles α and ϕ are the horizontal and vertical divergences, respectively, the first lying in the dispersion plane. The function G is the overall intensity profile of the x-ray source within its divergence, and J is its spectral composition. The functions $C_A(\cdot)$ and $C_B(\cdot)$ stand for the first and second crystal's reflection curves where their arguments are given by the expressions in brackets. The respective argument is the local incidence angle as function of divergence (α,ϕ) and rocking angle ω, minus the linear change of Bragg's angle Θ_A or Θ_B when λ deviates from the central wavelength λ_0. In the angular expression of crystal B, upper signs refer to anti-parallel $(n,+m)$-geometry commonly used as a spectrometer, whereas the lower signs refer to the parallel $(n,-m)$-geometry which is potentially a dispersion-less diffractometer.

3. Experimental setup

3.1 Si Kα X-ray source

The experiments employ the Kα doublet lines of Si (Z=14) [18] as given in tab. 1. They are generated in an x-ray tube (General Electric, phoenix sem|20) by focusing a 10 keV, 3 mA electron beam to 20 μm diameter onto a bulk Si anode, emitting both characteristic line emission (K and L-shell lines) and bremsstrahlung.

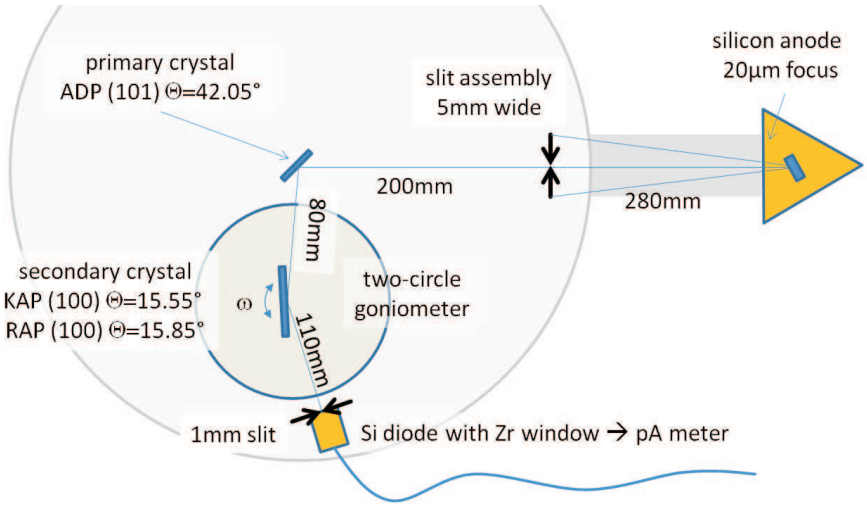

Figure 1. Experimental setup of the double crystal spectrometer. The primary ADP crystal selects the Si Kα doublet radiation from a Si fine focus x-ray tube. This radiation impinges onto a hydrogen phthalate sample mounted on the goniometer axis. The reflected x-rays are detected with a Si diode coupled to a pA-meter.

3.2 Crystal properties

In this work, the ideal $(n,-n)$-geometry could not be realized due to technical constraints of the vacuum chamber size and the in-vacuum goniometer dimensions. Instead, we realized a $(n,+m)$-setup as sketched in fig. 1.

Table 2 summarizes the x-ray properties for the employed crystals. Due to the high photo-absorption cross-section for soft x-rays, all three crystals show comparable absorption and extinction depths. For the KAP and RAP specimen, we note that the radiation penetrates less than $1\,\mu$m into the crystal surface.

In order to select only the Kα doublet of Si, a primary ADP crystal in orientation (101) is placed 480 mm from the anode inside a high vacuum tank (pressure $< 10^{-5}$ mbar) at a Bragg angle of $\Theta_A = 42.05°$. The initial divergence of the x-rays impinging onto the primary crystal is limited by a 5×5 mm wide slit assembly positioned 280 mm from the anode. In the dispersive plane, it is further limited by a 1 mm wide slit in front of the Si photo diode detector (± 0.8 mrad), while the vertical divergence is finally limited by its height of 5 mm (± 4 mrad).

3.3 Polarization of the x-rays

While the characteristic K-shell lines emitted from the tube are unpolarized, they exhibit a distinct polarization after being reflected by the primary crystal. The refractive index is approximately unity (the refraction correction amounts to only 53 seconds of arc), so that the intensities of the parallel and the perpendicular components at $\Theta_B = 42.05°$ are in the ratio of $P_\pi = \cos 2\Theta_B = 0.1$ to $P_\sigma = 1$. We may therefore consider the x-rays leaving the primary crystal to be dominantly (91%) σ-polarized.

Table 2. X-ray properties for ADP (101) and KAP/RAP (100) using Si Kα x-rays. Calculated values are according to the code DIXI [15]. The symmetric absorption depth is measured along the surface normal, and the extinction depth is for σ-polarized light.

		ADP	KAP	RAP
reflection		101	100	100
lattice constant 2d	[Å]	10.64	26.6	26.1
Bragg angle Θ_B	[°]	42.05	15.55	15.85
symmetric absorption depth	[μm]	2.38	1.12	0.98
extinction depth	[μm]	1.48	0.80	0.83

3.4 Double-crystal spectrometer

Within the initial divergence of $\sim 1^\circ$, the first ADP crystal reflects a spectral window of $\Delta E/E = \Delta\Theta/\tan\Theta \sim 1.6\%$. Hence the radiation reflected by the primary crystal has a divergence of $\sim 1^\circ$ and spans $\Delta E \sim 28\,\mathrm{eV}$ ($E = 1726 - 1754\,\mathrm{eV}$).

This radiation is subsequently used to study the reflectivity properties of RAP and KAP crystals, mounted alternatively as secondary crystals. As shown in fig. 1, the crystals are placed on the ω-circle of a two-circle in-vacuum goniometer, 80 mm from the primary ADP crystal. At a distance of 110 mm from the secondary crystal, a Si photo-diode is placed on the 2Θ-circle. The photo-current is measured with a pico-Ampère-meter (Keithley 617) and is proportional to the amount of detected x-rays. This diode is covered with a 200 nm Zr foil to suppress visible light. In order to obtain a measurement of the primary intensity I_0, the secondary crystal can be translated out of the goniometer center and the diode is positioned at $\Theta = 0^\circ$. For the final measurement, the diode detector is positioned at fixed $2\Theta_B$, while crystal angle is scanned around the Bragg angle Θ_B. The two goniometer circles and the pA-meter are controlled via a computer running LabView to automate the measurements.

In order to evaluate different experimental conditions, the triple-integral eq. 2.1 has been numerically solved. Since the x-ray tube emits isotropic, we may assume a uniform source intensity $G(\alpha,\phi) \equiv 1$ within the vertical divergence $\phi = \pm 4\,\mathrm{mrad}$ and the horizontal (dispersive) divergence $\alpha = \pm 0.8\,\mathrm{mrad}$, which enter as the limits of the first and third integration, respectively. The spectral composition of the source is modeled by two Lorentzians centered at $7.1255\,\text{Å}$ and $7.1280\,\text{Å}$ (widths of $0.49\,\mathrm{eV}$ according to Tab. 1) and integrating from $\lambda_{\min} = 7.01\,\text{Å}$ to $\lambda_{\max} = 7.24\,\text{Å}$. The central wavelength is chosen to coincide with the Kα_1 line.

The reflection curves of the primary and secondary crystals C_A and C_B are calculated using the code DIXI [15] as shown in the left panel of fig. 2. For C_B, we used the results for σ-polarized x-rays, but we note that at a Bragg angle of $\sim 15^\circ$ the differences for the two polarization states are subtle.

The results for parallel $(n,-m)$ and anti-parallel $(n,+m)$ configurations and for both KAP and RAP are shown in the right panel of fig. 2. Due to the unequal dispersions of the first and second crystals, neither setup is dispersion-free to allow measuring the shape of the rocking curve. In contrast, it exhibits the shape of the Kα doublet, confined by the slit settings. Also the anti-parallel setup (red curves) have a higher dispersion and the K-doublet is wider spaced than in the parallel setup (black curves). Oscillations in the curves are due to numerical artifacts. The intensity is

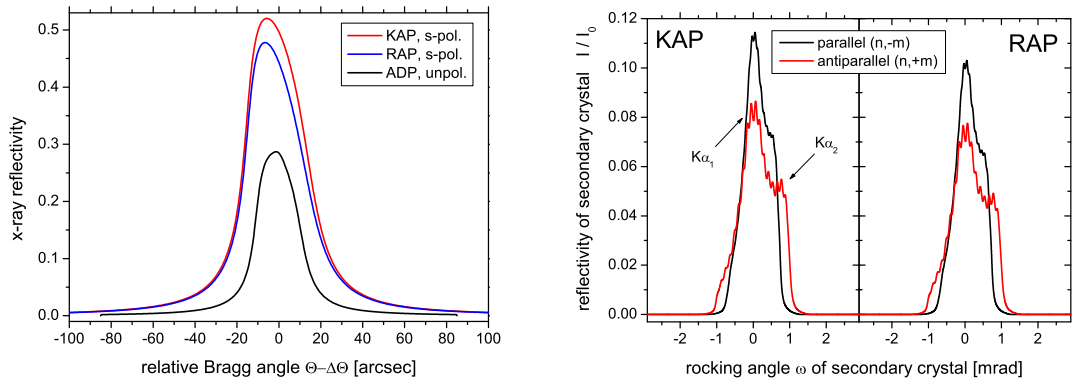

Figure 2. *Left:* Rocking curves for ADP, KAP and RAP at the Si Kα_1 photon energy and the relevant polarization states. The curves are calculated using the code DIXI [15]. *Right:* Numerical solution of the triple-integral for parallel and anti-parallel settings of ADP and KAP/RAP crystals. The theoretical rocking curves from DIXI have been assumed.

normalized to the amount of x-rays reflected by the first crystal, which is calculated via eq. 2.1, but using $C_B = 1$.

We note that the parallel setting yields higher peak reflectivities and narrower profiles as compared to the anti-parallel setting. When integrating the curves, both settings yield identical integrated reflectivities $R^{\sigma}_{\mathrm{int}} = 99.89\,\mu$rad and $89.7\,\mu$rad for KAP and RAP, respectively. Results for KAP show an increased reflectivity compared to RAP corresponding to their rocking curves (cf. left panel). We conclude that both setups allow measuring the integrated reflectivity of the secondary crystal.

4. Results

4.1 Reflection curves

Due to technical constrains, reflection curves for KAP and RAP could only be measured in $(n,+m)$-geometry, yielding the results shown in fig. 3. The secondary crystal is aligned to be as parallel as possible to the incoming x-rays ($\Theta \sim 0^\circ$) with a precision better than $\pm 0.5^\circ$. Therefore, the measured absolute Bragg angle shows an offset of about -0.4° with respect to the theoretical values (cf. tab. 2) due to the initial alignment. Both graphs show the same relative axes for better comparison.

4.2 Cleavage

In fig. 3, three curves are shown for each crystal. Each of these curves is composed from individual subsequent scans to avoid systematic drifts. The black curve is measured from a crystal which was stored in a clean environment at ambient (office) conditions for about 10 years. No special sealing under protective gas or vacuum was applied. The initial thickness was about 2 mm. The red curve shows the reflectivity of a crystal surface that was freshly cleaved by attaching a sticky tape to one

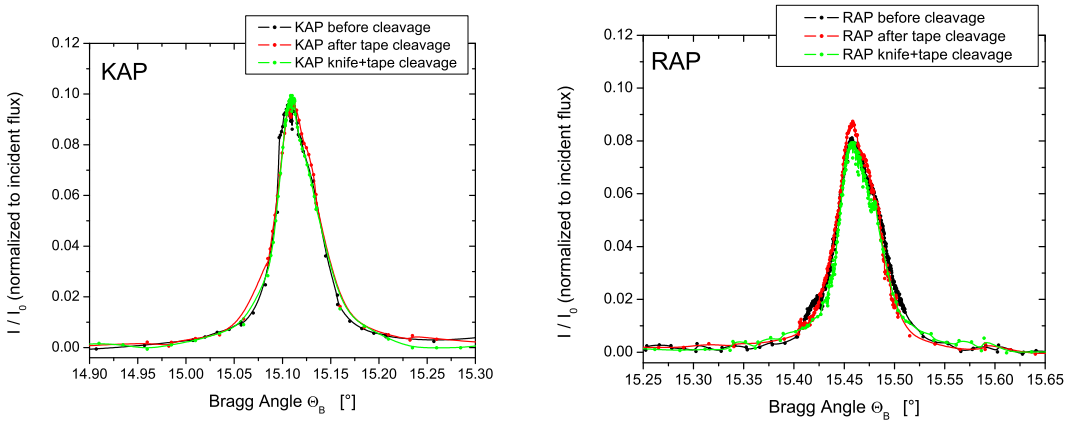

Figure 3. Measured reflection curves for RAP and KAP. The absolute value of the Bragg angle is offset with respect to the theoretical values due to uncertainties in the initial alignment when the crystal is placed parallel to the x-rays. Curves are shown for crystals before cleavage, after cleavage with tape, and after splitting the crystal with a knife and pulling it apart with tape.

entire surface and pulling it off. In this process, an about 10 μm thin surface layer sticks to the tape and is separated from the crystal bulk. Finally, the green curve is the reflectivity of a crystal surface that was prepared by inserting a sharp razor blade ~ 0.5 mm deep into the crystal, and then pulling the pieces apart using again sticky tape. Here, the crystal is split into two pieces of about 1 mm thickness each, exposing a fresh surface from bulk material.

4.3 Integrated reflectivity

We compare the measured integrated reflectivity, analyzed within the boundaries of the plots (fig. 3) and compare them to theoretical expectations for σ-polarized light (cf. tab. 3) and the numerical studies (cf. fig 2).

In the case of KAP, the average measured value of $R_{\mathrm{int}} \sim 105\,\mu$rad is only 3.5% higher than the the theoretical integrated reflectivity, assuming perfect crystals (dynamical limit) and σ-polarized light. For RAP, the average measured value of $R_{\mathrm{int}} \sim 87\,\mu$rad is only 4.4% lower than the the theoretical value. Reasons for this slight discrepancy, which lie within the error bar of the measurement, are possible crystal defects.

When comparing the measurements to the respective simulations (red curves in the right panel fig. 2), we note that the Kα doublet structure is washed out in the measurements, while peak and integrated reflectivity are in good agreement. This can be caused by the primary and secondary diffraction planes, as well as the slit in front of the diode, not being absolutely parallel.

5. Conclusions

The integrated x-ray reflectivity R_{int} of RAP and KAP crystals at a photon energy of (1740 ± 14) eV is studied using a (n,+m) double-crystal setup. The absolute measured reflectivities are in $\pm 5\%$ agreement with the values predicted by the dynamic diffraction theory for perfect crystals when

Table 3. Measured integrated reflectivities and theoretical values (calculated ones using DIXI [15]) for comparison. We recall that the radiation impinging onto the second crystal is dominantly σ-polarized. The integrated reflectivities $R^{\sigma}_{\rm int}$ are the values for σ-polarized light, given both for the dynamical limit (assuming an ideal perfect crystal) and the kinematic limit (ideal mosaic crystal). All values are in μrad.

case	before cleavage	tape cleavage	knife cleavage	mean value	$R^{\sigma}_{\rm int}$ dyn. lim.	$R^{\sigma}_{\rm int}$ kin. lim.
KAP	105 ± 4	110 ± 4	101 ± 4	105.3	102	159
RAP	88 ± 4	89 ± 4	85 ± 4	87.3	91	131

absorption is included. Within 4% error bars, specimen that were exposed to ambient conditions over many years show identical $R_{\rm int}$ compared to specimen that were cleaved just before the measurement. Further, no differences are observed between cleaving off a $10\,\mu$m surface layer and splitting the entire crystal bulk. We conclude that at 1.7 keV photon energy the penetration depth of $\sim 1\,\mu$m is large compared to a potentially deteriorated surface layer of a few 10 nm.

Potentially, hydrogen phthalate crystals can be employed for spectroscopy of significantly softer x-rays ($E_{\rm ph} > 480\,$eV) due to their large lattice spacing [8, 9]. For example, studying the Fe Lα line at $E_{\rm ph} = 708\,$eV ($\lambda = 1.75\,$nm) involves Bragg angles of $\sim 41^{\circ}$, but the radiation is absorbed in the first 250 nm, while the extinction depth is comparable to that of Si Kα case. Here, the ratio of a potentially deteriorated surface layer to the reflecting volume is less beneficial, and cleavage could improve the x-ray reflectivity.

Acknowledgments

We would like to thank I. Uschmann and O. Wehrhan for fruitful discussions about cleaving crystals, and R. Loetzsch for help with the LabView program. UZ is further grateful to the VolkswagenStiftung for his Peter-Paul-Ewald Fellowship. This work was partially funded by the German Helmholtz association via the Helmholtz Institute Jena, and the German Federal Ministry for Education and Research (BMBF) via priority programme FSP 302.

References

[1] SM Vinko, O Ciricosta, BI Cho, K Engelhorn, H-K Chung, CRD Brown, T Burian, J Chalupskỳ, RW Falcone, C Graves, et al. Creation and diagnosis of a solid-density plasma with an x-ray free-electron laser. *Nature*, 482(7383):59–62, 2012.

[2] T R Preston, S M Vinko, O Ciricosta, H-K Chung, R W Lee, and J S Wark. The effects of ionization potential depression on the spectra emitted by hot dense aluminium plasmas. *High Energy Density Physics*, 9(2):258–263, 2013.

[3] O Ciricosta, SM Vinko, H-K Chung, B-I Cho, CRD Brown, T Burian, J Chalupskỳ, K Engelhorn, RW Falcone, C Graves, et al. Direct measurements of the ionization potential depression in a dense plasma. *Physical review letters*, 109(6):065002, 2012.

[4] BI Cho, K Engelhorn, SM Vinko, H-K Chung, O Ciricosta, DS Rackstraw, RW Falcone, CRD Brown, T Burian, J Chalupskỳ, et al. Resonant k α spectroscopy of solid-density aluminum plasmas. *Physical review letters*, 109(24):245003, 2012.

[5] DS Rackstraw, SM Vinko, O Ciricosta, BI Cho, K Engelhorn, H-K Chung, CRD Brown, T Burian, J Chalupskỳ, RW Falcone, et al. Opacity effects in a solid-density aluminium plasma created by photo-excitation with an x-ray laser. *High Energy Density Physics*, 11:59–69, 2014.

[6] LS Birks and JM Siomkajlo. Long-spacing metal organic crystals for x-ray spectroscopy. *Spectrochimica Acta*, 18(3):363–366, 1962.

[7] SA Pikuz, VM Romanova, TA Shelkovenko, Tat'yana Aleksandrovna Pikuz, A Ya Faenov, E Förster, J Wolf, and O Wehrhan. Use of higher-order reflection from mica crystals in x-ray spectroscopic investigations at 0.1–0.3 nm. *Quantum Electronics*, 25(1):16, 1995.

[8] M Vollbrecht, O Treichel, I Uschmann, K Gäbel, R Lebert, and E Förster. Soft-x-ray imaging with toroidally curved thallium acid phthalate crystals in the water window. *Applied optics*, 37(10):1803–1807, 1998.

[9] A Galler. Bestimmung des spektralen Auflösungsvermögens im weichen Röntgengebiet. Master's thesis, Friedrich-Schiller University Jena, 2005.

[10] I. Uschmann, E. Förster, et al. X-ray reflection properties of elastically bent perfect crystals in Bragg geometry. *Journal of Applied Crystallography*, 26(3):405–412, jun 1993.

[11] G Hölzer, O Wehrhan, J Heinisch, E Förster, TA Pikuz, A Ya Faenov, SA Pikuz, VM Romanova, and TA Shelkovenko. Flat and spherically bent muscovite (mica) crystals for x-ray spectroscopy. *Physica Scripta*, 57(2):301, 1998.

[12] EJ Gamboa, DS Montgomery, IM Hall, and RP Drake. Imaging x-ray crystal spectrometer for laser-produced plasmas. *Journal of Instrumentation*, 6(04):P04004, 2011.

[13] U Zastrau, C R D Brown, et al. Focal aberrations of large-aperture HOPG von-Hàmos x-ray spectrometers. *Journal of Instrumentation*, 7(09):P09015, 2012.

[14] U Zastrau, A Woldegeorgis, E Förster, R Loetzsch, H Marschner, and I Uschmann. Characterization of strongly-bent HAPG crystals for von-Hámos x-ray spectrographs. *Journal of Instrumentation*, 8(10):P10006, 2013.

[15] G Hölzer, O Wehrhan, and E Förster. Characterization of Flat and Bent Crystals for X-ray Spectroscopy and Imaging. *Crystal Research and Technology*, 33(4):555–567, 1998.

[16] A H Compton and S K Allison. *X-rays in Theory and Experiment*, volume 18. van Nostrand New York, 1935.

[17] J A Bearden and J S Thomsen. The double-crystal X-ray spectrometer: corrections, errors, and alignment procedure. *Journal of Applied Crystallography*, 4(2):130–138, Apr 1971.

[18] G Zschornack. *Handbook of X-ray Data*, volume 1. Springer, 2006.